Ecotoxicology and Environmental Safety 273 (2024) 116104

Contents lists available at ScienceDirect

Ecotoxicology and Environmental Safety

journal homepage: www.elsevier.com/locate/ecoenv

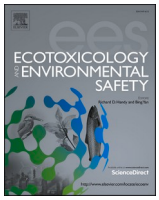

Ultrafine particulate matter pollution and dysfunction of endoplasmic reticulum Ca^{2+} store: A pathomechanism shared with amyotrophic lateral sclerosis motor neurons?

Silvia Sapienza [a], Valentina Tedeschi [a], Barbara Apicella [b], Anna Pannaccione [a], Carmela Russo [b], Maria Josè Sisalli [c], Giorgia Magliocca [a], Stefania Loffredo [c,d], Agnese Secondo [a,*]

[a] Department of Neuroscience, Reproductive and Odontostomatological Sciences, University of Naples Federico II, Naples 80131, Italy
[b] Istituto di Scienze e Tecnologie per l'Energia e la Mobilità Sostenibili (STEMS)-CNR, Naples 80125, Italy
[c] Department of Translational Medical Sciences, University of Naples Federico II, Naples 80131, Italy
[d] Center for Basic and Clinical Immunology Research (CISI), University of Naples Federico II, WAO Center of Excellence, Naples 80131, Italy

ARTICLE INFO

Handling Editor: Dr Yong Liang

Keywords:
Air pollution
Carbon PM
$[Ca^{2+}]i$ homeostasis
ER-stress
Neurotoxicity
SOCE

ABSTRACT

Increased risk of neurodegenerative diseases has been envisaged for air pollution exposure. On the other hand, environmental risk factors, including air pollution, have been suggested for Amyotrophic Lateral Sclerosis (ALS) pathomechanism. Therefore, the neurotoxicity of ultrafine particulate matter (PM0.1) (PM < 0.1 μm size) and its sub-20 nm nanoparticle fraction (NP20) has been investigated in motor neuronal-like cells and primary cortical neurons, mainly affected in ALS. The present data showed that PM0.1 and NP20 exposure induced endoplasmic reticulum (ER) stress, as occurred in cortex and spinal cord of ALS mice carrying G93A mutation in SOD1 gene. Furthermore, NSC-34 motor neuronal-like cells exposed to PM0.1 and NP20 shared the same proteomic profile on some apoptotic factors with motor neurons treated with the L-BMAA, a neurotoxin inducing Amyotrophic Lateral Sclerosis/Parkinson–Dementia Complex (ALS/PDC). Of note ER stress induced by PM0.1 and NP20 in motor neurons was associated to pathological changes in ER morphology and dramatic reduction of organellar Ca^{2+} level through the dysregulation of the Ca^{2+}-pumps SERCA2 and SERCA3, the Ca^{2+}-sensor STIM1, and the Ca^{2+}-release channels RyR3 and IP3R3. Furthermore, the mechanism deputed to ER Ca^{2+} refilling (e.g. the so called store operated calcium entry-SOCE) and the relative currents ICRAC were also altered by PM0.1 and NP20 exposure. Additionally, these carbonaceous particles caused the exacerbation of L-BMAA-induced ER stress and Caspase-9 activation. In conclusion, this study shows that PM0.1 and NP20 induced the aberrant expression of ER proteins leading to dysmorphic ER, organellar Ca^{2+} dysfunction, ER stress and neurotoxicity, providing putative correlations with the neurodegenerative process occurring in ALS.

1. Introduction

In recent years, more and more concerns have arisen about the health risk of atmospheric particulate matter (PM) due to motor vehicle and industrial emissions. Several current studies on the joint effects of air pollution focus on large-size PM fraction (PM10, PM < 10 μm). For instance, after air pollution inhalation, the 2 PM fractions with a well-recognized lung and cardiovascular toxicity are PM10 and PM2.5 (size< 2.5 μm) (Oberdörster et al., 2000; Mantecca. et al., 2010; Farina et al., 2011). Moreover, PM with fine (PM2.5, PM < 2.5 μm) and ultrafine (PM0.1, PM < 0.1 μm) sizes have a stronger ability to penetrate tissues deeply with a poor possibility to be cleared (Oberdörster et al., 1994, 2004; Oberdö Craig et al., 2008). In addition, exposure to the unmonitored PM0.1 particulate matter fraction is estimated to be very high (Schraufnagel, 2020). Compared to fine particles, PM0.1 is retained longer in the lung thus inducing more pulmonary inflammation (Schraufnagel, 2020). Of note, PM0.1 may affect the brain and its development (Calderon-Garciduenas et al., 2016; Block, Calderon-Garciduenas, 2009; You et al., 2022). In fact, brain translocation of ultrafine particulate matter can occur through an active passage across biological membranes, BBB leak, and/or olfactory bulb passage (Oberdorster, et al., 2004; Tian et al., 2019), a direct route to

* Corresponding author.
E-mail address: secondo@unina.it (A. Secondo).

https://doi.org/10.1016/j.ecoenv.2024.116104
Received 7 August 2023; Received in revised form 29 January 2024; Accepted 9 February 2024
Available online 19 February 2024

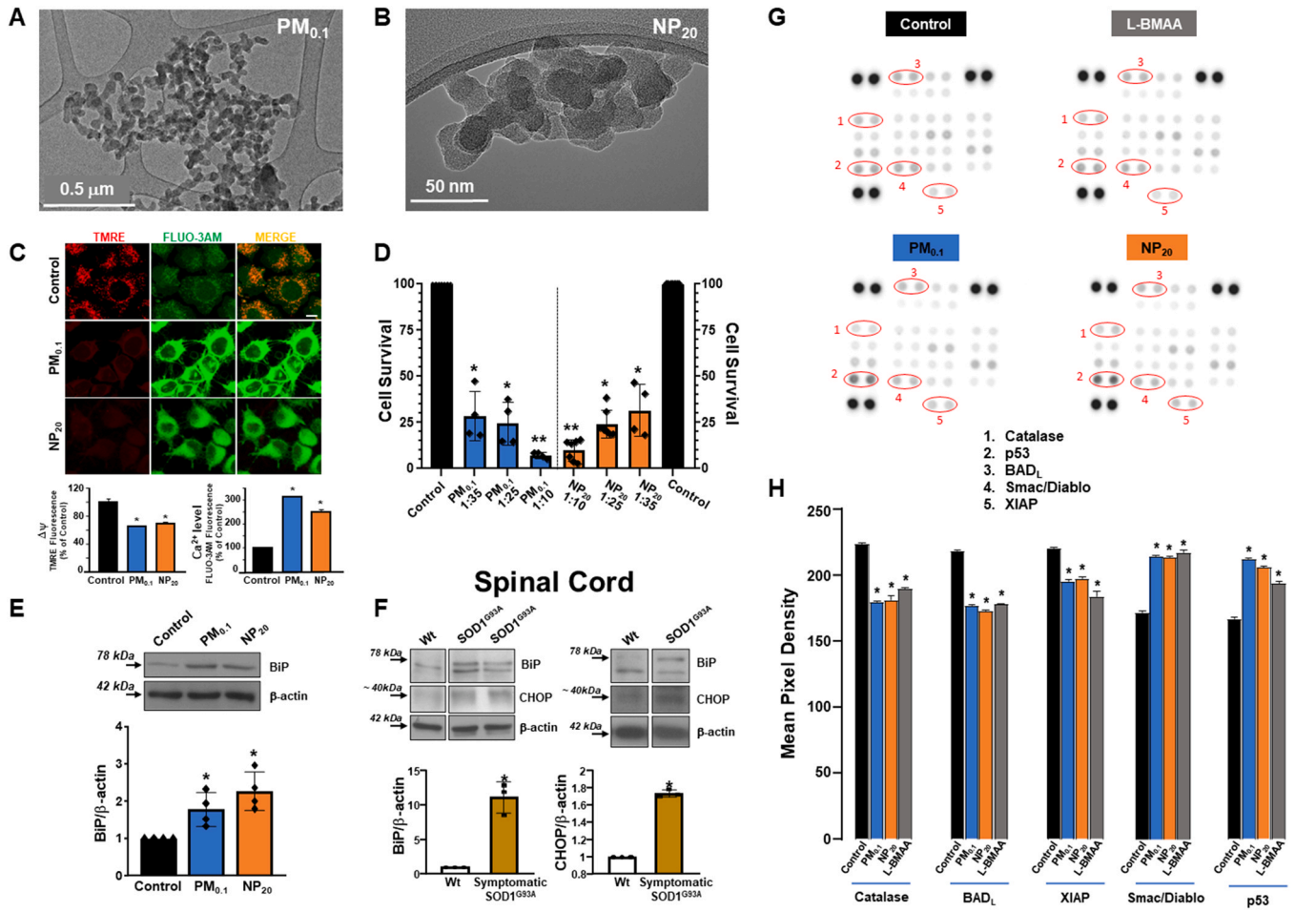

Fig. 1. PM0.1 and NP20 induced ER stress in motor neuronal NSC-34 cells and primary cortical neurons as occurred in symptomatic SOD1G93A ALS mice. (A, B) TEM and HRTEM images of PM0.1 and NP20, respectively. (C) Confocal images of TMRE- and Fluo-3AM-loaded NSC-34 cells exposed to PM0.1 and NP20 for 24 hrs measuring cell viability. Below: quantification of mitochondrial membrane potential as $\Delta\Psi$ N=40 cells) and intracellular Ca^{2+} level in the same cells as measure of cell viability. * $p < 0.05$ vs. respective controls. (D) Measurement of cell viability in NSC-34 motor neurons exposed to PM0.1 and NP20 at various concentrations (for reference 1:35 dilution corresponds to 2.86 ppm and 0.71 ppm for PM0.1 and NP20, respectively). Cell viability was measured as mitochondrial activity, since cell suffering corresponds to the reduction in mitochondrial activity. * $p < 0.05$ vs. controls, ** $p < 0.05$ vs. previous concentrations in each group. (E, F) Representative Western blotting and quantification of BiP expression in NSC-34 motor neuronal cells after 48 hrs exposure to PM0.1(1:35 dilution corresponding to 2.86 ppm) and NP20 (1:35 dilution corresponding to and 0.71 ppm) (E). * $p < 0.05$ vs. respective control; (F) Representative Western blottings and quantification of BiP and CHOP expression in Spinal Cord of Wt and SOD1G93A mice at 4.5 months of age (symptomatic ALS mice). *$p < 0.05$ vs. respective control. Double bands of BiP/GRP78 in Fig. F could be due to the presence of non-neuronal cells in mice brain lysates. Here, upper bands have been quantified. Data are means±SE of 4 (E) or 3 (F) separate experiments. * $p < 0.05$ vs. respective controls. (G) Representative blots of proteomic immunoassay from NSC-34 cells under control conditions or exposed to L-BMAA (300 μM/48hrs), PM0.1 (1:35 dilution corresponding to 2.86 ppm/48hrs), and NP20 (1:35 dilution corresponding to and 0.71 ppm/48hrs) (H) Quantification as reported in G. Data are means±SE of 3 separate experiments * $p < 0.05$ vs. respective control (vehicle- treated).

circumvent blood brain barrier in human (Oberdorster, et al., 2004; Tian, et al., 2019). Molecularly, PM0.1 exposure may induce oxidative stress and neuroinflammation in these brain areas with a consequent neurotoxicity and cognitive impairment (You et al., 2022). Increasing reports indicate that PM0.1 can trigger neurodegenerative diseases (Genc et al., 2012). Of note, its sub-20 nm nanoparticle fraction NP20, -whose emission is determined by the new technology combustion systems- cross the BBB more easily (Hartz et al., 2008). However, neither the involvement of NP20 nor the inherent molecular mechanism has been established for brain toxicity and neurodegenerative diseases. Of interest, Amyotrophic Lateral Sclerosis (ALS) has been recognized to have an environmental etiopathogenesis (Bozzoni, et al., 2016). Furthermore, two recent epidemiological researches have also established a long-term correlation between air pollution and ALS risk (Malek et al., 2015; Seelen et al., 2017). Of note, in the latter study, ALS has been associated with air pollutants produced by traffic (Seelen et al., 2017). Moreover, a new correlation between short-term exposure to PM2.5/PM10 and ALS has been also established (Myung et al., 2019). In the present study, the correlation between ultrafine PM fraction exposure and ALS has been investigated by exploring some relevant molecular mechanisms associated to Ca^{2+} dyshomeostasis that caused motor neuron loss in this type of neurodegeneration. To this aim, a complex approach based on biochemical and functional techniques' integration has been used in order to identify druggable molecular targets useful to arrest or, at least, reduce neurodegenerative progression. From a molecular point of view, ER stress pathway is considered as an essential pathomechanism of several neurodegenerative diseases triggered by neurotoxicants (Cannon and Greenamyre, 2011), including ALS (Jeon et al., 2023). Therefore, starting from the evidence that ER is affected in ALS motor neurons and it may represent one of its causative mechanisms, the effects of PM0.1 and NP20 have been investigated on ER stress, organellar Ca^{2+} homeostasis and ER machinery in motor neurons, the cell-type affected in ALS. The present data showed that the neuronal ER homeostasis was completely dysregulated by PM0.1 and NP20 that affected the expression and activity of ER Ca^{2+} sensor and channels. Collectively, the identification of a dysfunctional mechanism induced by

Table 1
List of antibodies used in the manuscript.

Antibody	Catalogue number	Supplier	Species	Type	Dilution	Already tested in
GRP78 (BiP)	#3183 (RRID: AB_10695864)	Cell Signaling Technology, Inc. (Danvers, MA, USA)	Rabbit	Polyclonal	1:1000	Tedeschi, V. *et al.*, 2019; Secondo, A. *et al.*, 2019
Caspase-12	#2202 (RRID: AB_2069200)	Cell Signaling Technology, Inc. (Danvers, MA, USA)	Rabbit	Polyclonal	1:1000	Petrozziello, T. *et al.*, 2017
CHOP	#2895 (RRID: AB_2089254)	Cell Signaling Technology, Inc. (Danvers, MA, USA)	Mouse	Monoclonal	1:1000	Ron, D. and Hebener, J.F., 1992
Anti-SERCA2 ATPase	#Ab2861 (RRID: AB_2061425)	Abcam (Cambridge, UK)	Mouse	Monoclonal	1:1000	Huang, J.P. *et al.*, 2020
Anti-SERCA3 ATPase	#ACP-014 (RRID: AB_2756568)	Alomone Labs (Jerusalem, Israel)	Rabbit	Polyclonal	1:1000	Tedeschi, V. *et al.*, 2021
Anti-STIM1	#ACC-063 (RRID: AB_2039893)	Alomone Labs (Jerusalem, Israel)	Rabbit	Polyclonal	1:1000	Secondo, A. *et al.*, 2019
β-Actin-Peroxidase	#A3854 (RRID: AB_262011)	Sigma-Aldrich (Milan, Italy)	Mouse	Monoclonal	1:10000	Tedeschi, V. *et al.*, 2021
Caspase 9 (cleaved Asp330)	#GTX132331 (RRID:AB_2886615)	GeneTex (Irvine, CA, USA)	Rabbit	Polyclonal	1:1000	Tedeschi et al., 2019
RyR3	#ARR-003 (RRID: AB_2040186)	Alomone Labs (Jerusalem, Israel)	Rabbit	Polyclonal	1:1000	Tedeschi, V. *et al.*, 2021
Anti-IP3R-3	#610313 (RRID: AB_397705)	BD Biosciences (CA, USA)	Mouse	Monoclonal	1:500	Tedeschi, V. *et al.*, 2021

ultrafine PM fraction exposure at neuronal level must draw attention to the negative impact that urban particulates have on human brain.

2. Material and methods

2.1. Ultrafine Particulate Isolation and characterization

In accordance to the recent literature on this field (Marcella et al., 2022), carbon PM was collected in a lab-scale combustion system, constituted of an atmospheric pressure, and a premixed ethylene/oxygen flame stabilized on a McKenna burner (Holthuis & Associates, CA, Sebastopol, California, USA). The experimental conditions employed for the flame, the sampling and the extraction and separation procedures were the same as reported in Sapienza et al., (2022). Briefly, PM was captured in this lab-scale combustion technique by placing a glass plate into the flame (Russo et al., 2020). Dimethyl sulfoxide (DMSO) was used to suspend the ultrafine particles PM0.1. Then, it was collected on the glass plate after its extraction in dichloromethane (DCM) in order to remove the soluble organic carbon (OC). PM0.1 was further filtered through 20 nm pore size Anotop filters (Whatman) to separate the smaller particles (NP20, which made up 25% of the total PM0.1 sample under the tested experimental conditions) from the larger fractions. Generally, it is considered that PM0.1 fraction constitutes only 1–8% of the mass of particulate matter (PM) in ambient air (Zhu and Hinds, 2002). However, as regards the number concentration of the total PM0.1 (not distinguishing between NP20 and NP >20 nm particles), values between 4.85×104 cm–3 and 1.80×105 cm–3 have been reported for locations affected by vehicular traffic (Schneider et al., 2015). Of note, the comparison between the distribution of the particles synthesised in laboratory by the actual procedure and those collected in the atmosphere showed a very good agreement in their respective parameters (Russo et al., 2023). Furthermore, previous investigations have reported an accurate characterisation of the OC and PM0.1 components. According to a previous study by Apicella et al., 2022, PAHs and high-molecular-weight aromatic species make up the majority of OC, while the PM0.1 fraction is particularly high in carbon with a low percentage of hydrogen (H/C atomic ratio is around 0.1) (Apicella et al., 2022). The structural characterization of PM0.1 and NP20 fractions has been performed by transmission electron microscopy (TEM) and high-resolution transmission electron microscopy (HRTEM). PM0.1 samples, preliminarily separated from the adsorbed organic compound by DCM and NP20 samples, after DMSO evaporation in an oven, were dispersed in ethanol by ultrasonic agitation and dropped onto carbon lacey grids for TEM and HRTEM analysis, respectively. An electron microscope operating at 200 kV was used to capture images of Fig. 1A and B.

2.2. Reagents and media

Cell culturing media and reagents used in the present study were purchased from Gibco (ThermoFisher Scientific Inc., Waltham, MA, USA), while ECL reagents and nitrocellulose membranes were from Cytiva Amersham (Amersham, UK).

Thapsigargin, the ATP bioluminescent assay kit, poly-D-lysine/poly-L-lysine, Ara-C and L-BMAA were purchased from Sigma-Aldrich (Milan, IT). Fura-2/AM, Fluo-3/AM and TMRE were from Molecular Probes (Invitrogen, ThermoFisher Scientific Inc., Waltham, MA, USA).

The CytoPainter ER Staining Kit was purchased from Abcam (Cambridge, UK).

2.3. Cell Cultures and treatments

2.3.1. Primary cortical neuron cultures

Primary cortical neurons were obtained from the cortex of 14/16-day-old Wistar rat embryos as reported in Secondo et al., (2019).

All procedures to isolate cortical neurons were performed according to protocols approved by the Ethical Committee of the "Federico II" University of Naples and by Italian Health Ministry.

2.3.2. Clonal motor neurons

Mouse motor-neuron-like hybrid cells (NSC-34) (Cashman et al., 1992) were grown as reported in Petrozziello et al., (2017). Most experiments were performed with PM0.1 at the concentration of 2.86 ppm and NP20 at the concentration of 0.71 ppm (1:35 dilution from each stock solution).

2.3.3. L-BMAA exposure as a model of ALS/PDC

The cyanobacterial β-N-methylamino-L-alanine (L-BMAA) is described as a low-potency excitotoxin increasing the incidence of amyotrophic lateral sclerosis (ALS) and Parkinsonism-dementia complex (PDC) in Guam. L-BMAA is produced by a variety of genera cyanobacteria and it may threaten human brain health crossing BBB. To mimic ALS/PDC, NSC-34 motor neurons were exposed to L-BMAA (300 μM /48 h). Under these conditions, L-BMAA promotes oxidative stress and ER stress (Petrozziello et al., 2017). Furthermore, some experiments were performed by exposing NSC-34 motor neurons to L-BMAA plus PM0.1 or NP20.

2.4. Animal model

In order to minimize animal suffering and reduce the number of animals used in the study, experiments on ALS mice were performed

following the international guidelines for animal research also approved by the Animal Care Committee of "Federico II" University of Naples, Italy and Italian Ministry of Health. SOD1G93A mouse -expressing high copy number of mutant human SOD1 with a Gly93Ala substitution- was obtained from Jackson Laboratories (Bar Harbor, ME, USA). SOD1-G93A transgenic mice are normally viable and fertile. According to the international literature in the field, this animal model phenotypically reproduces the symptoms of the human disease around the third/fourth month of life with weight loss and motor difficulties. This model is the only validated mouse model of ALS in accordance to the ALS Therapy Development Institute. The spinal cord and cortex tissues were extracted as reported in Anzilotti et al., (2021).

2.5. Western blotting

Sample supernatants, prepared as previously reported (Sapienza et al., 2022), were used for Western blotting analysis. Protein content was determined by Bradford method (Bradford, 1976). Antibodies were reported in Table 1.

2.6. Cell viability (MTT assay, mitochondrial membrane potential and intracellular calcium level)

In order to assess cell viability, neuronal cells were incubated with 3 [4,5-dimethylthiazol-2-yl]−2,5-diphenyl-tetrazolium bromide (0.5 mg/ml in PBS) for 1 hour at 37°C as reported in Secondo et al., (2007). The reduction of tetrazolium salts by dehydrogenases with primarily mitochondrial localization has been detected spectrophotometrically at 570 nm, once solubilized in DMSO. Therefore, MTT assay has been used to calculate the quantity of cells with active metabolism (Surin et al., 2017).

Mitochondrial membrane potential was measured in the "redistribution mode" by the lipophilic and cell permeable dye tetramethyl rhodamine ethyl ester (TMRE). After PM0.1 or NP20 treatment, motor neurons were loaded with TMRE (20 nM/30 min) and washed at the end of the incubation. Mitochondrial membrane depolarization was measured as decline in mitochondria-localized fluorescence intensity. Intracellular calcium level was detected simultaneously by Fluo-3AM. Confocal images were obtained with a Zeiss inverted 700 confocal laser scanning microscopy using a Xenon laser at the illumination minimum output of 0.5%.

2.7. ER Staining

The probe of the CytoPainter ER Staining Kit was incubated according to the manufacturer protocol on NSC-34 cells plated on precoated multiwells. Live images were then acquired with an Axiovert 5 (Carl Zeiss) and processed with the software Labscope (ZEISS Labscope, www.zeiss.com). Images were analysed through ImageJ (Fiji software).

2.8. $[Ca^{2+}]_i$ Measurements

$[Ca^{2+}]_i$ was measured by video-imaging on single-cell as reported in Secondo et al., (2019). SOCE measurements in motor neurons were performed with the Axiovert 200 microscope (Carl Zeiss) connected to MicroMax 512BFT cooled CCD camera (Princeton Instruments) using Meta-Morph/MetaFluor Imaging System software (Universal Imaging) as reported in Secondo et al., (2019). SOCE was measured depleting ER Ca^{2+} stores with the SERCA pump inhibitor thapsigargin (TG, 1 μM) in Krebs-Ringer saline solution (5.5 mM KCl, 160 mM NaCl, 1.2 mM MgCl2, 10 mM d-glucose, and 10 mM HEPES-NaOH, pH 7.4 + 0.5 mM EGTA). ER Ca^{2+} depletion is known to stimulate a rapid coupling between the ER Ca^{2+} sensor STIM1 and the plasma membrane channels involved in Ca^{2+} store refilling (i.e. ORAI channels). After ER depletion, the subsequent reintroduction of 3 mM Ca^{2+} allows SOCE detection as $[Ca^{2+}]_i$ increase.

2.9. Electrophysiology

Ca^{2+} release-activated Ca^{2+} currents (I_{CRAC}) were recorded by patch-clamp in whole-cell configuration with a 100-ms voltage ramp protocol (from +90 to −120 mV) from −15 mV holding potential every 10 s, as reported in Secondo et al., (2019). The external solutions contained (in mM) 145 NaCl, 5 KCl, 1 CaCl2, 1 MgCl2, 10 HEPES, and 10 glucose (pH 7.4), whereas the pipette solution contained (in mM) 145 CsCl, 8 NaCl, 10 MgCl2, 10 HEPES, 10 EGTA, and 2 Mg-ATP (pH 7.2). Since the CRAC channel and the L-type Ca^{2+} channel are both highly selective for Ca^{2+}, Nimodipine was added to block the L-type voltage-dependent Ca^{2+} channels. Furthermore, spermine chloride was also used to block Mg^{2+}-inhibitable currents while Tetraethylammonium and Tetrodotoxin were added to the external solution to block tetraethylammonium-sensitive K+ and tetrodotoxin-sensitive Na+ currents, respectively. ICRAC were normalized to membrane capacitance measured as pA/pF.

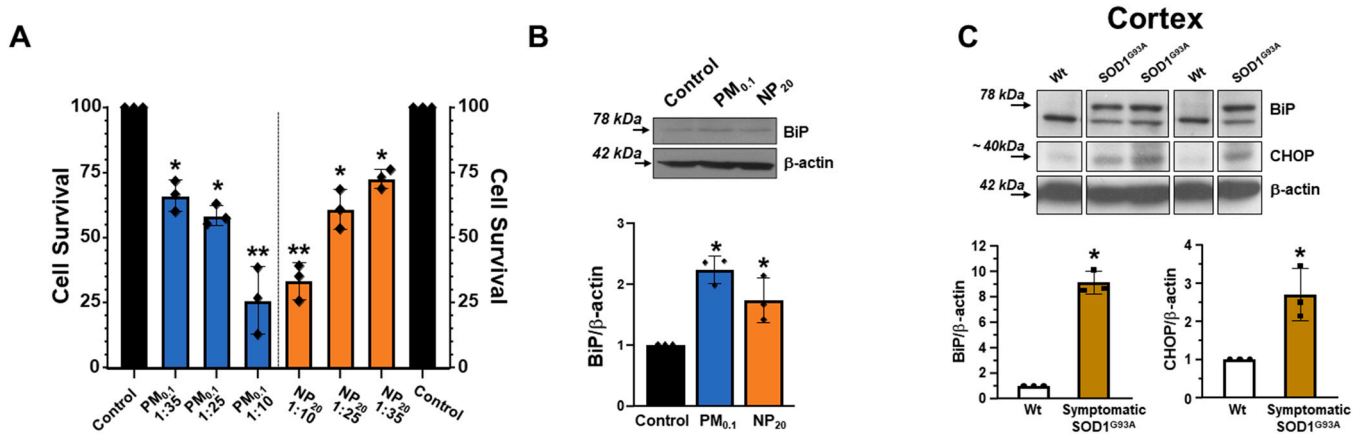

Fig. 2. ER stress in primary cortical neurons exposed to PM0.1 and NP20 and in brain cortex of symptomatic SOD1G93 A ALS mice. (A) Measurement of cell viability in mature primary cortical neurons exposed to PM0.1 and NP20 at various concentrations (for reference 1:35 dilution corresponds to 2.86 ppm and 0.71 ppm for PM0.1 and NP20, respectively). * $p < 0.05$ vs. controls, ** $p < 0.05$ vs. previous concentrations in each group. (B) Representative Western blotting and quantification of BiP expression in primary cortical neurons after 48 hrs exposure to PM0.1(1:35 dilution corresponding to 2.86 ppm) and NP20 (1:35 dilution corresponding to and 0.71 ppm). * $p < 0.05$ vs. respective control; (C) Representative Western blottings and quantification of BiP and CHOP expression in brain cortex of Wt and SOD1G93A mice at 4.5 months of age (symptomatic ALS mice). *$p < 0.05$ vs. respective controls. Data are means±SE of 3 separate experiments. * $p < 0.05$ vs. respective controls.

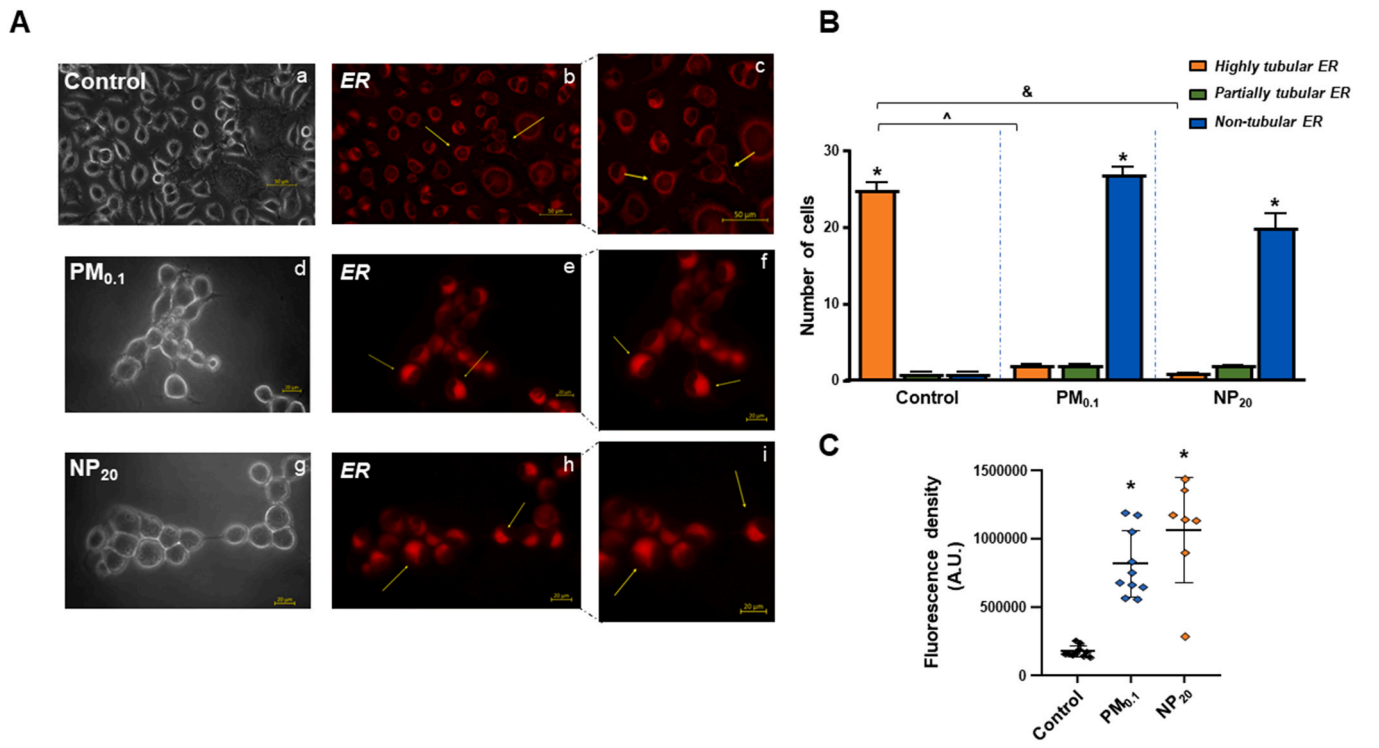

Fig. 3. PM0.1 and NP20 induced ER morphological changes in motor neuronal NSC-34 cells. (A) ER morphology in live motor neuronal cells stained with ER specific marker (see Material and Method's section) under control conditions (b, c) or exposed to PM0.1 (1:35 dilution corresponding to 2.86 ppm/48hrs) (e, f), and NP20 (1:35 dilution corresponding to and 0.71 ppm/48hrs) (h, i). The relative bright field images are reported in a, d and g, respectively. (B) Quantification of ER morphology in A (b, e and h) as "*Highly tubular ER*", "*Partially tubular ER*" *or* "*non-tubular ER*" under control conditions or exposed to PM0.1 and NP20. * $p < 0.05$ vs. all in each group (C) Fluorescence density of ER staining in A (b, e and h) measured as arbitrary units in at least 7 fields in each image by Image J software. Data are means±SE of 3 separate experiments * $p < 0.05$ vs. control (vehicle- treated).

2.10. Quantification of ATP content

ATP content was measured as index of mitochondrial and cell status. After boiling samples in 100 mM TRIS + 4 mM EDTA (pH 7.75), ATP level was measured by a bioluminescent assay using a standard luminometer.

2.11. Proteomic analysis on apoptotic proteins

After treatments, cell lysates were used to determine the effect of PM0.1 and NP20 on apoptotic-related proteins with proteomic analysis. The proteomic profile of motor neuronal cells was evaluated using a Proteome Profiler Mouse Apoptosis Array (R&D System, ARY031), a membrane-based sandwich immunoassay. Apoptosis-related proteins were visualised by chemiluminescence and protein levels were quantified relatively to their respective controls by ImageJ software.

2.12. Statistical analysis

Data were expressed as mean ± SE. Statistical analyses were performed with One-way ANOVA with Newman-Keuls's post-test or unpaired t-test, using GraphPad Prism 8 (GraphPad Software, La Jolla, CA, USA). Statistical significance was set at P values < 0.05.

3. Results and discussion

3.1. ER stress induced by PM0.1 and NP20 was a common pathomechanism shared with Amyotrophic Lateral Sclerosis tissues

Recent studies have suggested a relationship between endoplasmic reticulum (ER) stress and neurodegenerative processes in various disorders including amyotrophic lateral sclerosis (ALS) (Hetz and Saxena, 2017, Petrozziello et al., 2017). This mechanism impairs Ca^{2+} homeostasis and contributes to pathogenic protein aggregate accumulation during the neurodegenerative process. In order to acquire new mechanistic insights into the neurotoxicity induced by ultrafine PM0.1 and NP20, these carbonaceous particles were collected in a lab-scale combustion system as reported in the Material and Method's section. Once isolated, structural characterization of PM0.1 was performed by TEM (Fig. 1A) while that of NP20 was achieved by HRTEM (Fig. 1B). Then, some neuronal cultures mainly affected by ALS were exposed to these two types of tiny air pollutants capable of penetrating in few hours into the neurons (Sapienza et al., 2022). Either motor neuronal-like NSC-34 cells or primary cortical neurons displayed a progressive reduction in cell viability at different concentrations of PM0.1 and nanoparticles NP20 as measured by mitochondrial membrane depolarization and reduction in mitochondrial metabolic activity (Fig. 1C, 1D and Fig. 2A). Furthermore, PM0.1 and NP20 induced a significant protein overexpression of the molecular chaperone BiP/GRP78 (Fig. 1E and Fig. 2B), considered as an ER stress sensor (Kopp et al., 2019). In consideration of the role of ER stress in ALS, as proof of concept, a significant increase in protein expression of the two ER stress markers BiP/GRP78 and CHOP was detected in those brain areas containing motor neurons such as spinal cord and brain cortex of symptomatic ALS mice carrying the most common SOD1 mutation namely G93A (Fig. 1F and Fig. 2C, respectively). Furthermore, the proteomic profile of some proteins involved in oxidative stress and protective neuronal functions (i.e. catalase, BADL, XIAP), mitochondrial dysfunction and ER/mitochondria cross-talk (i.e. Smack/Diablo), and ER stress (i.e. p53) in NSC-34 motor neurons exposed to PM0.1 and NP20 mirrored that of motor neurons exposed to β-N-methylamino-L-alanine (L-BMAA) (Figs. 1G and 1H), the neurotoxin responsible for the Guamanian form of the disease named ALS/PDC (Petrozziello et al., 2017). These data are suggestive of a common detrimental mechanism shared by air-pollution-related neurotoxicity

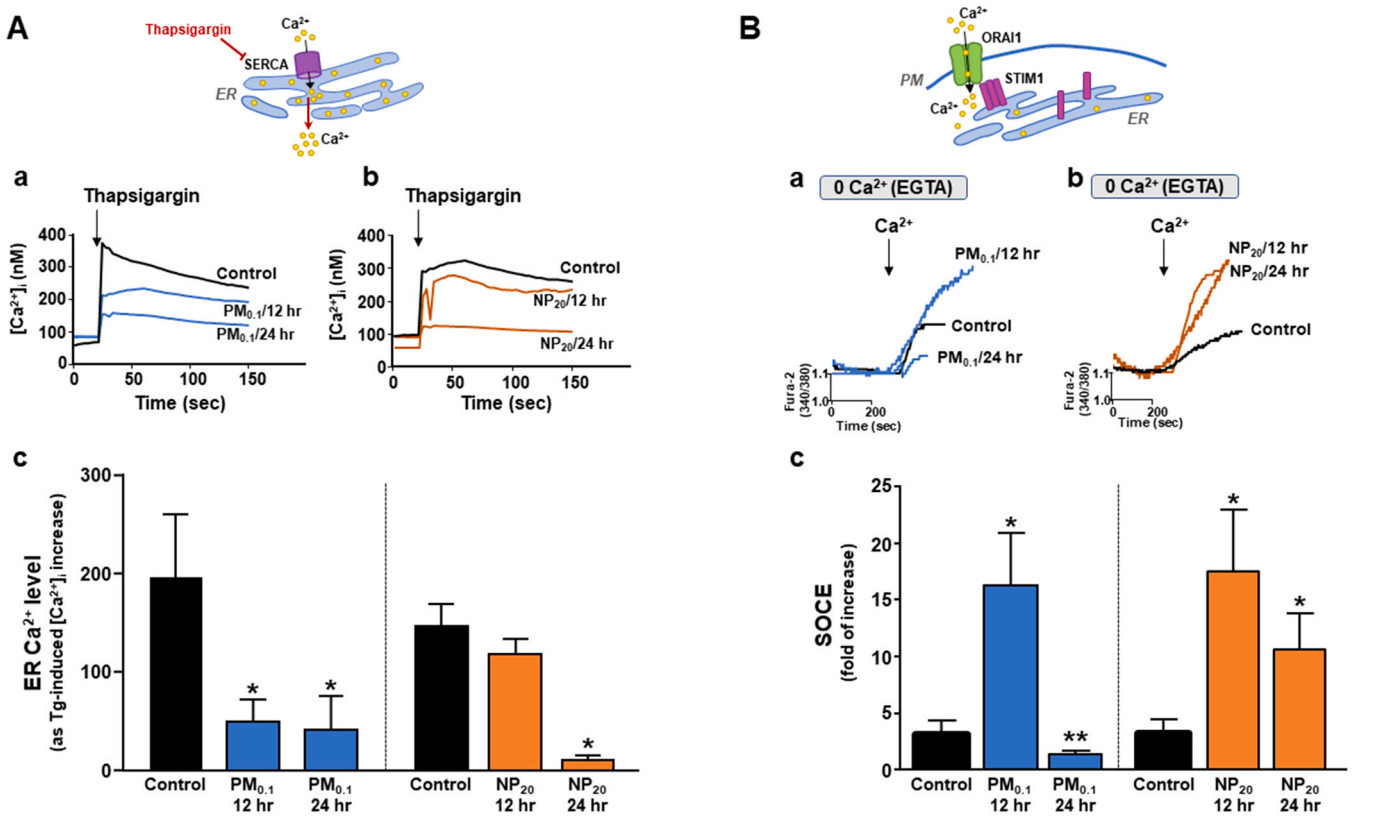

Fig. 4. PM0.1 and NP20 reduced Ca^{2+} content in ER modulating store-operated calcium entry (SOCE) mechanism in motor neuronal NSC-34 cells. (A a,b) Representative superimposed single-cell traces of the effect of 1 μM thapsigargin (Tg) on [Ca2+]i in Ca2+-free (0 Ca2+; 1.5 mM EGTA) under control conditions (black traces in a and b) and after 12 and 24 hrs PM0.1 (1:35, Blue traces in a) or NP20 (1:35, Orange traces in b). (A c) Quantification of A. Data are means±SE of 3 separate experiments * $p < 0.05$ vs. respective control. (B a,b) Representative superimposed single-cell traces of SOCE under control conditions (black traces in a and b) and after 12 and 24 h PM0.1 (1:35, Blue traces in a) or NP20 (1:35, Orange traces in b). To measure SOCE as [Ca2+]i, movement, neurons were exposed to thapsigargin in the absence of extracellular calcium and, then, re-exposed to 2 mmol/L Ca^{2+}. (B c) Quantification of B. Data are means±SE of 3 separate experiments * $p < 0.05$ vs. control. ** $p < 0.05$ vs. 12 hrs.

with ALS neurodegeneration.

3.2. Exposure to PM0.1 and NP20 induced a dramatic reduction of ER Ca^{2+} level

Endoplasmic reticulum (ER) represents the most important organelle storing Ca^{2+} and one of the main subcellular components controlling protein folding, whose activity is necessary for motor neuron life and function (Bernard-Marissal et al., 2018). Another important ER function is represented by the maintenance of ionic gradients modulating the mobilization and cycling of synaptic vesicles in the axons; this is an energetically demanding process due to the functional relationship with mitochondria (Brini et al., 2014). Therefore, ER Ca^{2+} homeostasis should be perfectly maintained to ensure the motor neuron function. For this reason, the effect of PM0.1 or NP20 has been tested on ER morphology and Ca^{2+} level (Fig. 3, Figure S1A, and Fig. 4). The extent of pathological changes of ER morphology in PM0.1- and NP20-treated motor neurons was studied by the fluorescent staining of the organelle. It was quantified as a significant increase in the percentage of cells showing non-tubular ER against the greater percentage of cells with highly tubular ER detected in control conditions (Fig. 3A, B). Furthermore, quantitative fluorescence analysis of dye-tagged ER in NSC-34 motor neurons showed that PM0.1 and NP20 induced a higher increase in the basal fluorescence than in cells under control conditions (Fig. 3C).

Time-course of PM0.1 exposure showed that it was able to drastically reduce ER Ca^{2+} level already after 12 hrs of incubation, maintaining this detrimental reduction thereafter (Fig. 4a,c). On the other hand, the effect of NP20 was more progressive, leaving unchanged the ER Ca^{2+} level after 12 hrs of exposure and determining its drastic reduction after 24 hrs (Fig. 4a,b,c). Moreover, the ER Ca^{2+} replenishment occurs through the activation of store operated calcium entry (SOCE) that is continuously stimulated by organellar depletion (Putney, 2013). Mechanistically, SOCE is due to the interaction between STIM proteins sensing Ca^{2+} into ER and Ca^{2+} channels in the plasma membrane (Cahalan, 2009; Hewavitharana et al., 2007). Therefore, SOCE was measured by Ca^{2+}-imaging technique eliciting the calcium-induced calcium release (CICR) mechanism by thapsigargin in a Ca^{2+}-free solution followed by Ca^{2+} reintroduction in Fura-2-loaded motor neurons previously exposed to PM0.1 or NP20 (Fig. 4B). Time-course of PM0.1 exposure showed that SOCE significantly increased after 12 hrs of exposure while reduced thereafter (Fig. 4B a, c). However, SOCE increased in the presence of NP20 after 12 hr of incubation remaining significantly higher than control after 24 hrs (Fig. 4 b,c). That ER Ca^{2+} level remained stably low after 24 hrs in the presence of an increased SOCE mechanism in those cells exposed to air pollutants, suggests that several elements of ER machinery were functionally compromised. Therefore, we further investigated on this aspect.

3.3. PM0.1 and NP20-induced ER Ca^{2+} level reduction was due to the organellar machinery dysfunction

Stromal interaction molecule 1 (STIM1), an essential ER transmembrane protein sensing ER Ca^{2+} by its Ca^{2+}-binding EF hand, plays a pivotal role in the store-operated Ca^{2+} entry phenomenon through the association with the plasma membrane channels (Ambudkar et al.,

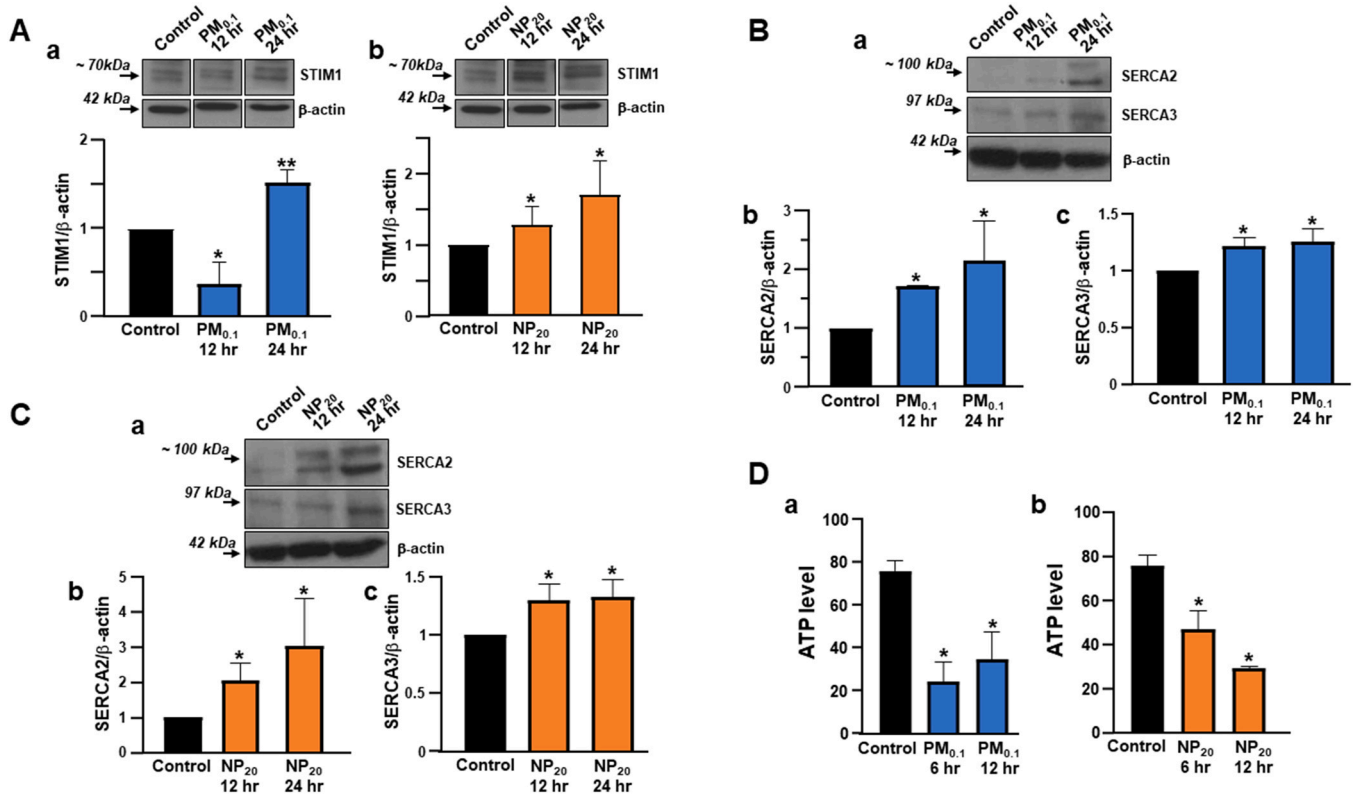

Fig. 5. PM0.1 and NP20 induced changes in ER proteins involved in Ca2+ sensing and handling (i.e. STIM1, SERCA2, and SERCA3). (A) Western blots and quantification of STIM1 expression in NSC-34 cells after 12 and 24 hrs exposure to PM0.1 in "a" (1:35 corresponding to 2.86 ppm) or NP20 in "b" (1:35 corresponding to 0.71 ppm). Data are means±SE of 4 separate experiments. * $p < 0.05$ vs. respective controls. ** $p < 0.05$ vs. 12 hrs PM. (B, C) Western blots and quantification of SERCA2 (B, a,b; C,a,b) and SERCA3 (B, a, c; C, a,c) expression in NSC-34 cells after 12 and 24 hrs exposure to PM0.1 in "B" (1:35 corresponding to 2.86 ppm) or NP20 in "C" (1:35 corresponding to 0.71 ppm). Data are means±SE of 5 separate experiments. * $p < 0.05$ vs. respective controls. (D) ATP level in NSC-34 cells after 6 and 12 hrs exposure to PM0.1 in "a" or NP20 in "b". Data are means±SE of 3 separate experiments. * $p < 0.05$ vs. respective controls.

2017). Therefore, SOCE depends on STIM1 sensing function (Hooper et al., 2013). In the attempt to study the compromission of this mechanism, the effect of PM0.1 and NP20 was studied on STIM1 protein expression in motor neuronal cells. Moreover, STIM1 protein expression was significantly reduced in motor neuronal cells exposed to PM0.1 for 12 hrs while it increased after 24 hrs of PM0.1 exposure compared with control (Fig. 5A). NP20 produced a strong increase in STIM1 protein expression only after 24 hrs of exposure (Fig. 5A). Of note, STIM1 is the unique mechanism by which ER Ca^{2+} reduction can be detected by the cell thus regulating Ca^{2+} entry across the plasma membrane. It is noteworthy that, after SOCE activation, ER Ca^{2+} entry is mediated by the SERCA pump, an ATPase that transfers Ca^{2+} ions from the cytosol to the SR/ER lumen via ATP hydrolysis (Andersen and Vilsen, 1998; MacLennan, 2000; Vandecaetsbeek et al., 2009; Brini et al., 2013; Valentim et al., 2022). Therefore, the effect of PM0.1 and NP20 on SERCA2 and SERCA3, mainly expressed in the brain (Baba-Aissa et al., 1998; Brini and Carafoli, 2009), was explored in motor neurons. Protein expression of SERCA2 and SERCA3 was significantly upregulated at 12 and 24 hrs either by PM0.1 or NP20 exposure (Fig. 5B and C). Moreover PM0.1 and NP20 significantly affected ATP level very early: in fact, after 6 hrs of incubation, ATP level was significantly curtailed by both these air pollutants (Fig. 5D), thus hampering the ability of SERCAs to move Ca^{2+} inside the organelle. On the light of these results, the overexpression of STIM1 in the presence of ultrafine particulate matter and its nanoparticles may be interpreted as a compensatory mechanism to overcome the detrimental reduction of Ca^{2+} into ER.

3.4. Long-term exposure to PM0.1 and NP20 downregulated Icrac and SOCE in motor neuron-like cells

Upon ER Ca^{2+} leak, SOCE is responsible for ER Ca^{2+} refilling through the activation of the Ca^{2+} release-activated Ca^{2+} current (I_{CRAC}), a non-voltage activated and inwardly rectifying current (Golovina et al., 2001). Of note, STIM1 senses ER Ca^{2+} leak allowing the activation of I_{CRAC} and SOCE to refill Ca^{2+} after its own oligomerization (Luik et al., 2008).

After 48 hrs exposure to PM0.1 and NP20, a time point in which ATP is drastically reduced (Sapienza et al., 2022), ER Ca^{2+} channels and protein machinery moving Ca^{2+} were completely dysregulated: SOCE was drastically reduced compared with control (Fig. 6a,b) while STIM1 protein expression was upregulated in motor neurons exposed to ultrafine PM and nanoparticles (Fig. 6A c). In accordance to the effect of PM0.1 and NP20 on SOCE-mediated [Ca2+]i, patch-clamp experiments showed that I_{CRAC} measured at −120 mV was drastically reduced compared with control currents (Fig. 6B). Furthermore, after 48 hrs, a significant upregulation for SERCA2 and SERCA3 protein expression also occurred in the same experimental conditions (Fig. 6C a-f) as well as those of the ER release Ca^{2+} channels RyR3 and IP3R3 (Fig. 6D a-c). As a consequence of ER dysfunction and Ca^{2+} loss, active form of Caspase 12 protein was significantly upregulated by PM0.1 and NP20 long exposure (Fig. 6 E a-c). Of note, exposure to PM0.1 and NP20 together with the neurotoxin L-BMAA enhanced Caspase-9 protein expression (Fig. 6 d,e), thereby demonstrating the ability of ultrafine PM to interfere with ALS mechanisms. Moreover, only PM0.1 was able to potentiate the increased expression of BiP by L-BMAA (Supplementary: Figure S1B). This is in line with the neurotoxic effect of ultrafine PM, its nanoparticle component and its putative role in neurodegeneration. Moreover, the

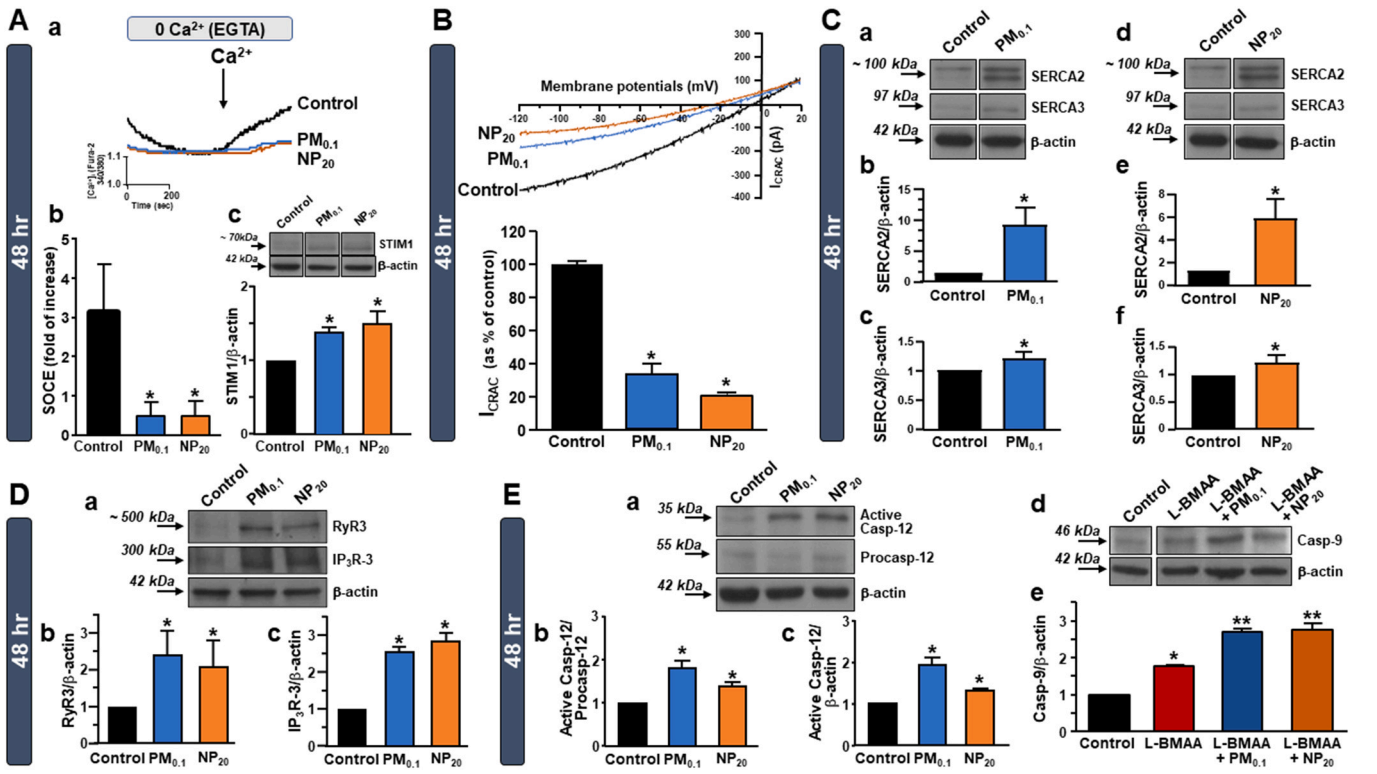

Fig. 6. Long exposure to PM0.1 and NP20 downregulated SOCE and I_{CRAC} modifying ER machinery and activating ER stress. (a,b) Representative superimposed single-cell traces of SOCE (at least 30 cells for each group) and quantification under control conditions (black trace) and after 48 hrs exposure to PM0.1 1:35 (Blue trace) or NP20 1:35 (Orange trace). (A c) Western blot and quantification of STIM1 expression in NSC-34 cells after 48 hrs exposure to PM0.1 (1:35 corresponding to 2.86 ppm) or NP20 (1:35 corresponding to 0.71 ppm). Data are means±SE of 4 separate experiments. * $p < 0.05$ vs. respective controls. (B) Whole-cell recordings and quantification of ICRAC in NSC-34 motor neurons under control conditions and after exposure to PM0.1 1:35 (Blue trace) or NP20 1:35 (Orange trace). Data are means±SE of 3 separate experiments (5–8 cells for each group). *$p<0.05$ vs control. (C) Western blots and quantification of SERCA2 (a,b,d,e) and SERCA3 (a,d,c,f) expression in NSC-34 cells after 48 hrs exposure to PM0.1 (1:35 corresponding to 2.86 ppm) or NP20 (1:35 corresponding to 0.71 ppm). Data are means±SE of 5 separate experiments. * $p < 0.05$ vs. respective controls. (D) Western blotting and quantification of RyR3 and IP3R-3 in NSC-34 cells under control conditions and after exposure to PM0.1 or NP20 (both at 1:35 dilution). Data are means±SE of 4 separate experiments. * $p < 0.05$ vs. respective controls. (E) Western blot and quantification of active Caspase 12 and procaspase-12 in NSC-34 cells exposed to PM0.1 or NP20 (both at 1:35 dilution/48hrs) (a-c) and Caspase-9 in NSC-34 cells exposed to L-BMAA alone or L-BMAA + PM0.1 or NP20 (both at 1:35 dilution/48hrs) (d, e). Data are means±SE of 3 separate experiments. *$p<0.05$ vs control. **$p<0.05$ vs L-BMAA and control.

upregulation of SERCAs and STIM1 proteins could be interpreted as compensatory mechanism in response to the longer exposure to PM0.1 and NP20, since SOCE was significantly downregulated after 48 hrs of treatment. Point of interest includes the upregulation of ER release Ca^{2+} channels RyR3 and IP3R3 after the exposure to PM0.1 and NP20 that could be considered as one of the main causative mechanisms of Ca^{2+} loss and ER stress.

Collectively, these data indicate that PM0.1 and NP20 determined a serious dysfunction of the main plasma membrane and ER mechanisms that are deputed to maintain ER Ca^{2+} homeostasis thus affecting motor neuronal life and functions. This cellular setting was characterized by several compensatory mechanisms due to an early curtailing effect on ATP level associated to a significant disruption of mitochondria. This impacts the activity of the cellular ATPases. Furthermore, due to the cross talk between mitochondria and ER, Ca^{2+} homeostasis resulted to be completely dysfunctional in motor neurons as occurs in neurodegenerative diseases. Therefore, the present study clearly established ER Ca^{2+} store dysregulation as a new mechanism underlying PM-induced neurotoxicity.

4. Conclusions

Atmospheric particulate matter (PM) is considered as the main contributor to the global burden of diseases associated with air pollution. PM of anthropogenic origin is associated to motor vehicle and industrial emissions, comprehending almost all the fine (PM2.5, size < 2.5 μm) up to ultrafine (PM0.1, size < 0.1 μm) particulate matter fractions. The alarmingly unmonitored PM0.1 and, in particular, its sub-20 nm fraction (i.e. NP20) can enter the brain and be uptaken by neurons, thus highlighting a strict association with neurodegeneration through organellar dysfunction. In the present study we showed that PM0.1 and NP20, collected in a lab-scale combustion system, showed toxic effects on endoplasmic reticulum (ER) function in motor neurons. Accordingly, they induced ER stress by disrupting ER morphology and ER Ca^{2+} handling function. This latter feature was due to the ER Ca^{2+} leak provoked by both PM0.1 and NP20 exposure followed by the progressive dysfunction of the ER refilling mechanisms, namely SOCE and ICRAC. Furthermore, under these conditions, the expression of the unique ER Ca^{2+} sensor STIM1 was dysfunctional together with SERCA pumps -deputed to organellar Ca^{2+} reuptake- and the main ER Ca^{2+}-releasing channels (i.e. IP3R3 and RyR3). In addition, SERCA activity was certainly compromised, since ATP production was rapidly reduced. This confirmed the detrimental effect of ultrafine PM on mitochondria. Of note, ER stress is considered as a common pathomechanism shared by several neurodegenerative diseases and, in particular, by ALS whose occurrence has been associated to environmental causes. As proof of concept, the significant increase in the ER stress markers BiP and CHOP was detected in those brain areas containing motor neurons such as brain cortex and spinal cord of symptomatic ALS mice carrying the most common SOD1 mutation, namely SOD1G93A. Furthermore, motor

neurons exposed to PM0.1 and NP20 showed the same proteomic profile of some apoptotic factors displayed by L-BMAA -treated motor neurons, a model to reproduce Guamanian form of ALS. Of interest, PM0.1 and NP20 enhanced ER stress and caspase-9 activation induced by L-BMAA.

Therefore, the present study showed a new mechanism underlying the neurotoxicity of anthropogenic ultrafine PM and its nanofraction NP20 that was shared by ALS and that could be therapeutically targeted to reduce or, at least treat, air pollution-induced neurotoxicity.

Funding

This work was supported by Progetto FRA (CdA_54_2020_FRA to A. S.), #NEXTGENERATIONEU (NGEU) and funded by the Ministry of University and Research (MUR), National Recovery and Resilience Plan (NRRP), project MNESYS (PE0000006) – A Multiscale integrated approach to the study of the nervous system in health and disease (DN. 1553 11.10.2022) to A.S. and A.P., and Progetto Fondazione Roche per la Ricerca Indipendente 2021 (57254) to V.T.

CRediT authorship contribution statement

Magliocca Giorgia: Data curation. **Loffredo Stefania:** Writing – original draft. **Pannaccione Anna:** Methodology, Data curation. **Russo Carmela:** Methodology, Conceptualization. **Tedeschi Valentina:** Methodology, Formal analysis, Data curation. **Apicella Barbara:** Writing – original draft, Resources, Methodology, Data curation. **Secondo Agnese:** Writing – review & editing, Writing – original draft, Methodology, Conceptualization. **Sapienza Silvia:** Methodology, Data curation, Conceptualization. **Sisalli Maria Josè:** Data curation, Formal analysis, Methodology.

Declaration of Competing Interest

The authors declare that they have no known competing financial interests or personal relationships that could have appeared to influence the work reported in this paper.

Data availability

Data will be made available on request.

Acknowledgments

We thank Professor Neil Cashman for the gift of NSC-34 cells.

Appendix A. Supporting information

Supplementary data associated with this article can be found in the online version at doi:10.1016/j.ecoenv.2024.116104.

References

Ambudkar, I.S., de Souza, L.B., Ong, H.L., 2017. TRPC1, Orai1, and STIM1 in SOCE: friends in tight spaces. Cell Calcium 63, 33–39. https://doi.org/10.1016/j.ceca.2016.12.009.

Andersen, J.P., Vilsen, B., 1998. Structure-function relationships of the calcium binding sites of the sarcoplasmic reticulum Ca(2+)-ATPase. Acta Physiol. Scand. Suppl. 643, 45–54.

Anzilotti, S., Valsecchi, V., Brancaccio, P., Guida, N., Laudati, G., Tedeschi, V., Petrozziello, T., Frecentese, F., Magli, E., Hassler, B., Cuomo, O., Formisano, L., Secondo, A., Annunziato, L., Pignataro, G., 2021. Prolonged NCX activation prevents SOD1 accumulation, reduces neuroinflammation, ameliorates motor behavior and prolongs survival in a ALS mouse model. Neurobiol. Dis. 159, 105480 https://doi.org/10.1016/j.nbd.2021.105480.

Apicella, B., Russo, C., Carpentieri, A., Tregrossi, A., Ciajolo, A., 2022. PAHs and fullerenes as structural and compositional motifs tracing and distinguishing organic carbon from soot. Fuel 309, 122356.

Baba-Aissa, F., Raeymaekers, L., Wuytack, F., Dode, L., Casteels, R., 1998. Distribution and isoform diversity of the organellar Ca2+ pumps in the brain. Mol. Chem. Neuropathol. 33, 199–208. https://doi.org/10.1007/BF02815182.

Bernard-Marissal, N., Chrast, R., Schneider, B.L., 2018. Endoplasmic reticulum and mitochondria in diseases of motor and sensory neurons: a broken relationship? Cell Death Dis. 9, 333. https://doi.org/10.1038/s41419-017-0125-1.

Block, M.L., Calderon-Garciduenas, L., 2009. Air pollution : mechanisms of neuro-inflammation and CNS disease. Trends Neurosci. 32, 506–516. https://doi.org/10.1016/j.tins.2009.05.009.

Bozzoni, V., Pansarasa, O., Diamanti, L., Nosari, G., Cereda, C., Ceroni, M., 2016. Amyotrophic lateral sclerosis and environmental factors. Funct. Neurol. 31, 7–19. https://doi.org/10.11138/fneur/2016.31.1.007.

Bradford, M.M., 1976. A rapid and sensitive method for the quantitation of microgram quantities of protein utilizing the principle of protein-dye binding. Anal. Biochem. 72, 248–254. https://doi.org/10.1006/abio.1976.9999.

Brini, M., Carafoli, E., 2009. Calcium pumps in health and disease. Physiol. Rev. 89, 1341–1378. https://doi.org/10.1152/physrev.00032.2008.

Brini, M., Calì, T., Ottolini, D., Carafoli, E., 2013. The plasma membrane calcium pump in health and disease. FEBS J. 280, 5385–5397. https://doi.org/10.1111/febs.12193.

Brini, M., Calì, T., Ottolini, D., Carafoli, E., 2014. Neuronal calcium signaling: function and dysfunction. Cell. Mol. Life Sci. 71, 2787–2814. https://doi.org/10.1007/s00018-013-1550-7.

Cahalan, M.D., 2009. STIMulating store-operated Ca(2+) entry. Nat. Cell Biol. 11, 669–677. https://doi.org/10.1038/ncb0609-669.

Calderon-Garciduenas, L., Leray, E., Heydarpour, P., Torres-Jardon, R., Reis, J., 2016. Air pollution, a rising environmental risk factor for cognition, neuro-inflammation and neurodegeneration: the clinical impact on children and beyond. Rev. Neurol. 172, 69–80. https://doi.org/10.1016/j.neurol.2015.10.008.

Cannon, J.R., Greenamyre, J.T., 2011. The role of environmental exposures in neurodegeneration and neurodegenerative diseases. Toxicol. Sci. 124, 225–250. https://doi.org/10.1093/toxsci/kfr239.

Cashman, N.R., Durham, H.D., Blusztajn, J.K., Oda, K., Tabira, T., Shaw, I.T., Dahrouge, S., Antel, J.P., 1992. Neuroblastoma x spinal cord (NSC) hybrid cell lines resemble developing motor neurons. Dev. Dyn. 194, 209–221. https://doi.org/10.1002/aja.1001940306.

Craig, L., Brook, J.R., Chiotti, Q., Croes, B., Gower, S., Hedley, A., Krewski, D., Krupnick, A., Krzyzanowski, M., Moran, M.D., Pennell, W., Samet, J.M., Schneider, J., Shortreed, J., Williams, M., 2008. Air pollution and public health: a guidance document for risk managers. J. Toxicol. Environ. Health A. 71, 588–698. https://doi.org/10.1080/15287390801997732.

Farina, F., Sancini, G., Mantecca, P., Gallinotti, D., Camatini, M., Palestini, P., 2011. The acute toxic effects of particulate matter in mouse lung are related to size and season of collection. Toxicol. Lett. 202, 209–217. https://doi.org/10.1016/j.toxlet.2011.01.031.

Genc, S., Zadeoglulari, Z., Fuss, S.H., Genc, K., 2012. The adverse effects of air pollution on the nervous system. J. Toxicol. 2012, 782462 https://doi.org/10.1155/2012/782462.

Golovina, V.A., Platoshyn, O., Bailey, C.L., Wang, J., Limsuwan, A., Sweeney, M., Rubin, L.J., Yuan, J.X., 2001. Upregulated TRP and enhanced capacitative Ca(2+) entry in human pulmonary artery myocytes during proliferation. Am. J. Physiol. Heart Circ. Physiol. 280, H746–H755. https://doi.org/10.1152/ajpheart.2001.280.2.H746.

Hartz, A.M.S., Bauer, B., Block, M.L., Hong, J.S., Miller, D.S., 2008. Diesel exhaust particles induce oxidative stress, proinflammatory signaling, and P-glycoprotein up-regulation at the blood-brain barrier. FASEB J. 22, 2723–2733. https://doi.org/10.1096/fj.08-106997.

Hetz, C., Saxena, S., 2017. ER stress and the unfolded protein response in neurodegeneration. Nat. Rev. Neurol. 13, 477–491. https://doi.org/10.1038/nrneurol.2017.99.

Hewavitharana, T., Deng, X., Soboloff, J., Gill, D.L., 2007. Role of STIM and orai proteins in the store-operated calcium signaling pathway. Cell Calcium 42, 173–182. https://doi.org/10.1016/j.ceca.2007.03.009.

Hooper, R., Samakai, E., Kedra, J., Soboloff, J., 2013. Multifaceted roles of STIM proteins. Pflug. Arch. 465, 1383–1396. https://doi.org/10.1007/s00424-013-1270-8.

Jeon, Y.M., Kwon, Y., Lee, S., Kim, H.J., 2023. Potential roles of the endoplasmic reticulum stress pathway in amyotrophic lateral sclerosis. Front. Aging Neurosci. 15, 1047897 https://doi.org/10.3389/fnagi.2023.1047897.

Kopp, M.C., Larburu, N., Durairaj, V., Adams, C.J., Ali, M.M.U., 2019. UPR proteins IRE1 and PERK switch BiP from chaperone to ER stress sensor. Nat. Struct. Mol. Biol. 26, 1053–1062. https://doi.org/10.1038/s41594-019-0324-9.

Luik, R.M., Wang, B., Prakriya, M., Wu, M.M., Lewis, R.S., 2008. Oligomerization of STIM1 couples ER calcium depletion to CRAC channel activation. Nature 454, 538–542. https://doi.org/10.1038/nature07065.

MacLennan, D.H., 2000. Ca2+ signalling and muscle disease. Eur. J. Biochem. 267, 5291–5297. https://doi.org/10.1046/j.1432-1327.2000.01566.x.

Malek, A.M., Barchowsky, A., Bowser, R., Heiman-Patterson, T., Lacomis, D., Rana, S., Youk, A., Talbott, E.O., 2015. Exposure to hazardous air pollutants and the risk of amyotrophic lateral sclerosis. Environ. Pollut. 197, 181–186. https://doi.org/10.1016/j.envpol.2014.12.010.

Mantecca, P., Farina, F., Moschini, E., Gallinotti, D., Gualtieri, M., Rohr, A., Sancini, G., Palestini, P., Camatini, M., 2010. Comparative acute lung inflammation induced by atmospheric PM and size-fractionated tire particles. Toxicol. Lett. 198, 244–254. https://doi.org/10.1016/j.toxlet.2010.07.002.

Marcella, S., Apicella, B., Secondo, A., Palestra, F., Opromolla, G., Ciardi, R., Tedeschi, V., Ferrara, A.L., Russo, C., Galdiero, M.R., Cristinziano, L., Modestino, L., Spadaro, G., Fiorelli, A., Loffredo, S., 2022. Size-based effects of anthropogenic

ultrafine particles on activation of human lung macrophages. Environ. Int. 166, 107395 https://doi.org/10.1016/j.envint.2022.107395.
Myung, W., Lee, H., Kim, H., 2019. Short-term air pollution exposure and emergency department visits for amyotrophic lateral sclerosis: a time-stratified case-crossover analysis. Environ. Int. 123, 467–475. https://doi.org/10.1016/j.envint.2018.12.042.
Oberdörster, G., Ferin, J., Lehnert, B.E., 1994. Correlation between particle size, in vivo particle persistence, and lung injury. Suppl 5(Suppl 5). Environ. Health Perspect. 102, 173–179. https://doi.org/10.1289/ehp.102-1567252.
Oberdörster, G., Finkelstein, J.N., Johnston, C., Gelein, R., Cox, C., Baggs, R., Elder, A.C., 2000. Acute pulmonary effects of ultrafine particles in rats and mice. Res. Rep. Health Eff. Inst. 96, 5–74.
Oberdörster, G., Sharp, Z., Atudorei, V., Elder, A., Gelein, R., Kreyling, W., Cox, C., 2004. Translocation of inhaled ultrafine particles to the brain. Inhal. Toxicol. 16, 437–445. https://doi.org/10.1080/08958370490439597.
Petrozziello, T., Secondo, A., Tedeschi, V., Esposito, A., Sisalli, M., Scorziello, A., Di Renzo, G., Annunziato, L., 2017. ApoSOD1 lacking dismutase activity neuroprotects motor neurons exposed to beta-methylamino-L-alanine through the Ca2+/Akt/ERK1/2 prosurvival pathway. Cell Death Differ. 24, 511–522. 10.1038/cdd.2016.154.
Putney, J.W., 2013. Alternative forms of the store-operated calcium entry mediators, STIM1 and Orai1. Curr. Top. Membr. 71, 109–123. https://doi.org/10.1016/B978-0-12-407870-3.00005-6.
Russo, C., Apicella, B., Tregrossi, A., Oliano, M.M., Ciajolo, A., 2020. Thermophoretic sampling of large PAH (C $\geq$ 22–24) formed in flames. Fuel 263, 116722.
Russo, C., Apicella, B., Ciajolo, A., 2023. Hydrogen, sp2 carbon hybridization, and sp2 clustering as pieces of the puzzling nanostructure of soot: a closer look. Energy Fuels 37, 12525–12540. https://doi.org/10.1021/acs.energyfuels.3c01194.
Sapienza, S., Tedeschi, V., Apicella, B., Palestra, F., Russo, C., Piccialli, I., Pannaccione, A., Loffredo, S., Secondo, A., 2022. Size-based effects of anthropogenic ultrafine particles on lysosomal TRPML1 channel and autophagy in motoneuron-like cells. Int. J. Mol. Sci. 23, 13041. https://doi.org/10.3390/ijms232113041.
Schneider, I.L., Calesso Teixeira, E., Silva Oliveira, L.F., Wiegand, F., 2015. Atmospheric particle number concentration and size distribution in a traffic–impacted area. Atmos. Pollut. Res. 5, 877–885. https://doi.org/10.5094/APR.2015.097.
Schraufnagel, D.E., 2020. The health effects of ultrafine particles. Exp. Mol. Med. 52, 311–317. https://doi.org/10.1038/s12276-020-0403-3.
Secondo, A., Staiano, R.I., Scorziello, A., Sirabella, R., Boscia, F., Adornetto, A., Valsecchi, V., Molinaro, P., Canzoniero, L.M., Di Renzo, G., Annunziato, L., 2007. BHK cells transfected with NCX3 are more resistant to hypoxia followed by reoxygenation than those transfected with NCX1 and NCX2: Possible relationship with mitochondrial membrane potential. Cell Calcium 42, 521–535. https://doi.org/10.1016/j.ceca.2007.01.006.
Secondo, A., Petrozziello, T., Tedeschi, V., Boscia, F., Vinciguerra, A., Ciccone, R., Pannaccione, A., Molinaro, P., Pignataro, G., Annunziato, L., 2019. ORAI1/STIM1 Interaction intervenes in stroke and in neuroprotection induced by ischemic preconditioning through store-operated calcium entry. Stroke 50, 1240–1249. https://doi.org/10.1161/STROKEAHA.118.024115.
Seelen, M., Toro Campos, R.A., Veldink, J.H., Visser, A.E., Hoek, G., Brunekreef, B., van der Kooi, A.J., de Visser, M., Raaphorst, J., van den Berg, L.H., Vermeulen, R.C.H., 2017. Long-term air pollution exposure and amyotrophic lateral sclerosis in Netherlands: a population-based case-control study. Environ. Health Perspect. 125, 097023 https://doi.org/10.1289/EHP1115.
Surin, A.M., Sharipov, R.R., Krasil'nikova, I.A., Boyarkin, D.P., Lisina, O.Yu, Gorbacheva, L.R., Avetisyan, A.V., Pinelis, V.G., 2017. Disruption of functional activity of mitochondria during MTT assay of viability of cultured neurons. Biochem. Mosc. 82, 737–749. https://doi.org/10.1134/S0006297917060104.
Tian, L., Shang, Y., Chen, R., Bai, R., Chen, C., Inthavong, K., Tu, J., 2019. Correlation of regional deposition dosage for inhaled nanoparticles in human and rat olfactory. Part. Fibre Toxicol. 16, 6. https://doi.org/10.1186/s12989-019-0290-8.
Valentim, M.A., Brahmbhatt, A.N., Tupling, A.R., 2022. Skeletal and cardiac muscle calcium transport regulation in health and disease. Biosci. Rep. 42, BSR20211997.
Vandecaetsbeek, I., Trekels, M., De Maeyer, M., Ceulemans, H., Lescrinier, E., Raeymaekers, L., Wuytack, F., Vangheluwe, P., 2009. Structural basis for the high Ca2+ affinity of the ubiquitous SERCA2b Ca2+ pump. Proc. Natl. Acad. Sci. 106, 18533–18538.
You, R., Ho, Y.S., Chang, R.C., 2022. The pathogenic effects of particulate matter on neurodegeneration: a review. J. Biomed. Sci. 29, 15. https://doi.org/10.1186/s12929-022-00799-x.
Zhu, Y., Hinds, W.C., 2002. Concentration and size distribution of ultrafine particles. J. Air Waste Manag. Assoc. 52, 1032–1042.